MethodsX 12 (2024) 102565

Contents lists available at ScienceDirect

MethodsX

journal homepage: www.elsevier.com/locate/methodsx

Visualization of rat tendon in three dimensions using micro-Computed Tomography

Destinee M. Ditton[a], Colin R. Marchus[a], Aimee L. Bozeman[b], Alleyna C. Martes[b], Michele R. Brumley[b], Nathan R. Schiele[a,*]

[a] Chemical & Biological Engineering, University of Idaho, 875 Perimeter Dr. MS 0904, Moscow, ID 83844, USA
[b] Psychology, Idaho State University, 921 S 8th Avenue Stop 8087, Pocatello, ID 83209, USA

ARTICLE INFO

Method name:
Contrast enhancing for tendon visualization by micro-CT

Keywords:
Tendon
Micro-CT
Imaging
Soft tissue

ABSTRACT

Micro-computed tomography (CT) is an X-ray-based imaging modality that produces three-dimensional (3D), high-resolution images of whole-mount tissues, but is typically limited to dense tissues, such as bone. The X-rays readily pass-through tendons, rendering them transparent. Contrast-enhancing chemical stains have been explored, but their use to improve contrast in different tendon types and across developmental stages for micro-CT imaging has not been systematically evaluated. Therefore, we investigated how phosphotungstic acid (PTA) staining and tissue hydration impacts tendon contrast for micro-CT imaging. We showed that PTA staining increased X-ray absorption of tendon to enhance tissue contrast and obtain 3D micro-CT images of immature (postnatal day 21) and sexually mature (postnatal day 50) rat tendons within the tail and hindlimb. Further, we demonstrated that tissue hydration state following PTA staining significantly impacts soft tissue contrast. Using this method, we also found that tail tendon fascicles appear to cross between fascicle bundles. Ultimately, contrast-enhanced 3D micro-CT imaging will lead to better understanding of tendon structure, and relationships between the bone and soft tissues.

- Simple tissue fixation and staining technique enhances soft tissue contrast for tendon visualization using micro-CT.
- 3D tendon visualization in situ advances understanding of musculoskeletal tissue structure and organization.

* Corresponding author.
E-mail address: nrschiele@uidaho.edu (N.R. Schiele).

https://doi.org/10.1016/j.mex.2024.102565
Received 5 September 2023; Accepted 9 January 2024
Available online 10 January 2024

Specifications table

Subject area:	Engineering
More specific subject area:	Bioimaging
Name of your method:	Contrast enhancing for tendon visualization by micro-CT
Name and reference of original method:	K.M. Lesciotto, S.M. Motch Perrine, M. Kawasaki, T. Stecko, T.M. Ryan, K. Kawasaki, J.T. Richtsmeier, Phosphotungstic acid-enhanced microCT: Optimized protocols for embryonic and early postnatal mice, Developmental Dynamics. 249 (2020) 573–585. https://doi.org/10.1002/dvdy.136. J. Sartori, S. Köhring, H. Witte, M.S. Fischer, M. Löffler, Three-dimensional imaging of the fibrous microstructure of Achilles tendon entheses in Mus musculus, J. Anat. 233 (2018) 370–380. https://doi.org/10.1111/joa.12837.
Resource availability:	Bruker SkyScan 1275 micro-CT scanner (Bruker, Kontich, Belgium). NRecon (v.2.0.0.5; Bruker microCT, Kontich, Belgium). CTvox (v.3.3; Bruker microCT, Kontich, Belgium). PTA (Sigma-Aldrich, Catalog # 79690, St. Louis, MO).

Introduction

Micro-computed tomography (CT) has been widely used to visualize X-ray opaque tissues, such as bone [1–4]. Micro-CT scanners transmit X-rays through a tissue and an X-ray detector measures their intensity, which is impacted by the tissue density and the X-rays that are absorbed. The resulting X-ray images are recorded as two-dimensional (2D) trans-axial projections [1,5–7]. After each projection is recorded, the sample is rotated by a predetermined magnitude (rotated through 180° if symmetrical or 360° if asymmetrical) until the sample has been fully imaged. The 2D projections are then digitally processed into a stack of transverse slices to create a 3D representation. The resulting 3D micro-CT images can display the density gradients throughout a sample, allowing for quantification of various structural components. This powerful imaging technology results in high-resolution (e.g., < 4 μm) and 3D rendering of bone with limited tissue pre-processing to enable analysis of both microscale (e.g., trabecular structures) and whole bone architecture [8–11]. While micro-CT has advanced bone imaging, a challenge with this imaging modality is that the surrounding soft tissues (e.g., tendon, muscle, cartilage, etc.) are not readily visualized due to their low tissue density and limited X-ray absorbance [12,13]. Therefore, there is a need to develop methods that capture the advantages of micro-CT to visualize the soft tissues as well as bone. Herein, we describe and validate a staining technique that targets the tendon for micro-CT imaging.

Tendon is highly collagenous and connects muscle to bone. Tendon is mainly composed of collagen type I and organized in a hierarchical structure. In the large multi-muscle tendons, such as the Achilles, this hierarchical structure consists of tropocollagens (~1.5 nm in diameter) that are bundled to form microfibrils (~3.5 nm in diameter), which are arranged into collagen fibrils (~50–500 nm in diameter) and then collagen fibers (10–50 μm in diameter). The collagen fibers are bundled to form fascicles (~50–400 μm in diameter), which are arranged into sub-tendon (~3–6 mm in diameter) and lastly the whole tendon (~10 mm in diameter) [14]. Tail tendons have a similar hierarchical structure but appear to have some more distinct primary collagen fiber bundles (sub-fascicles, ~20–400 μm in diameter), secondary fiber bundles (fascicles, ~150–1000 μm in diameter), and tertiary fiber bundles (~1–3 mm in diameter) [15–21]. These structural components can vary in size and quantity depending on the tendon and species [15–21]. Tendon is frequently injured and there are few options for repair. A challenge for improving tendon repairs is a limited understanding of normal tendon formation and the underlying structure-function relationships that allow for efficient force transfer between muscle and bone. Therefore, an enhanced understanding of the tendon structure and its anatomical relationship with adjacent tissues is needed. However, current imaging modalities for tendons have some limitations. For example, traditional histology is labor intensive and requires the generation of numerous tissue slices for staining and imaging where native configuration may be lost, especially across a whole limb. Further, traditional histology cannot be readily rendered in 3D, limiting an understanding of anatomical relationships [22–24]. Similarly, while other microscope-based techniques enable imaging of the underlying collagen structure, they have a relatively small field of view, making imaging the tendon from the muscle-insertion to the bone-insertion not practical. These challenges coupled with the advantages of micro-CT motivate the need to develop techniques to visualize tendon in 3D using micro-CT.

A potential solution to the low soft tissue density and limited X-ray absorption is to stain soft tissues with a compound that has higher density than the tissue of interest. Over 28 different contrast-enhancing stains were previously evaluated to increase soft tissue contrast for micro-CT imaging [25]. A mouse patellar tendon was visible with nine of these stains ($(NH_4)_2MoO_4$, $Ba(ClO_3)_2$, $HgCl_2$, Na_2WO_4, lead nitrate, acetate, phosphomolybdic acid (PMA), phosphotungstic acid (PTA) and $BaCl_2$), and the highest contrast intensity was found with PTA, PMA, and $HgCl_2$ [25]. However, the techniques did not evaluate if substructures of the tendon (e.g., fascicles) were visible or how tissue hydration state impacted soft tissue contrast. More recently, two high density stains were evaluated for soft tissue visualization by micro-CT, Lugol's iodine (I2KI) and PTA [23,25–27]. The effectiveness of these two stains appeared to depend on tissue type. I2KI improved skeletal muscle and vascular tissue contrast with micro-CT, while PTA appeared more effective with collagen-rich soft tissues [28–30]. I2KI penetrated tissues rapidly, compared to PTA or PMA, but I2KI lacked the ability to reveal substructures within highly collagenous tissues [26,31]. Further, I2KI resulted in some tissue shrinkage which may impact anatomical relationships [32]. While, both I2KI and PTA show promise for improving the soft tissue contrast in micro-CT, PTA appears to be especially promising based on its ability to bind with collagen more effectively than I2KI and reduced impact on tissue structure [33–37]. Additional studies found that PTA improved micro-CT imaging of tendon [32,38,39]. However, a current challenge is the lack of a systematic protocol that clearly demonstrates the conditions where PTA improves tendon contrast and if PTA can be used across different tendon types and levels of maturation, which impact collagen levels. Furthermore, there is limited understanding of how tendon hydration state impacts the PTA-induced micro-CT contrast [23,40–42]. However, a recent study found that critically

drying tendons can result in improved soft-tissue contrast, but a rehydrated state was not characterized [43]. Therefore, there was a need to develop and test a staining method to enhance tendon X-ray density and evaluate impacts of tissue hydration to improve contrast for micro-CT imaging.

The objective of this study was to develop a method to visualize tendon *ex vivo* in its native anatomical configuration in 3D using micro-CT. Therefore, we evaluated PTA as a contrast-enhancing stain as well as determined the impacts of the tissue hydration state (e.g., hydrated and dehydrated) on the visualization of tendon. We evaluated this method using whole-mount sections of tails and whole-mount hindlimbs in both immature (postnatal day 21) and sexually mature (postnatal day 50) rats. Overall, we demonstrated a simple method which enhances the contrast of tendon, which can be used to advance understanding of the native tendon anatomy and its relationship with the adjacent soft tissues and bone.

Methods details

Tissue isolation and fixation

Tails and hindlimbs were obtained from male and female postnatal day (P) 21 and P50 Sprague-Dawley rats. Rats were bred and maintained in accordance with NIH [44] and institutional animal care and use committee guidelines at Idaho State University. On P21 and P50 following euthanasia, whole P21 rat tails ($n = 7$) and hindlimbs ($n = 4$) and whole P50 rat tails ($n = 3$) and hindlimbs ($n = 3$) were isolated and soaked in Dulbecco's phosphate buffered saline (PBS, no calcium or magnesium; Gibco, Grand Island, NY, Catalog# 14–190–250), wrapped in gauze, frozen, and then shipped to the University of Idaho. After thawing in PBS at room temperature, the tails and hindlimbs were skinned using dissecting scissors and tweezers, but otherwise left intact. Tissues were then placed into 15 mL (P21) and 50 mL (P50) conical tubes with 10% neutral buffered formalin in PBS and fixed for 7–10 days at 4 °C on an orbital shaker. Tendons were then washed three times (5 min each) with PBS, and then stored in PBS at 4 °C.

Serial dehydration, staining and rehydration of tails and hindlimbs

All the following procedures occurred on an orbital shaker at 4 °C, unless otherwise noted. P21 tails ($n = 4$) and hindlimbs ($n = 4$) underwent serial dehydration, over 3 days, to 70% ethanol/30% water. For serial dehydration, tissues were treated with 30% ethanol in PBS for 1 day, then 50% ethanol in PBS for 1 day, and lastly 70% ethanol in distilled water for 1 day [23]. Once in 70% ethanol/30% water, the tissues were stained in a 2.5% w/v PTA (Sigma-Aldrich, St. Louis, MO, Catalog # 79690) solution in 70% ethanol for 10 days. Concentrations of ethanol and PTA were based on a review of prior studies [23,38,39,41,45–47]. Previous studies using high concentrations of PTA (≥5%) saw improved contrast for imaging, but were accompanied by tissue shrinkage [23,38,45]. To reduce the potential for tissue shrinkage, a lower concentration of PTA (2.5%) was utilized in combination with the serial dehydration steps in ethanol [39,41,45–47]. The PTA staining time does not appear to result in overstaining, but the incubation time should be long enough to ensure the tissue is completely penetrated by the stain (this can be checked with a rapid micro-CT scan, which is described below). The PTA solution can be made in a solution of water or ethanol, but an aqueous solution requires agitation to improve solubility (10–15 min at room temperature) [48]. The 2.5% PTA-70% ethanol solution was changed to provide fresh solution every 3–4 days. After 10 days, all tails were cut to a more manageable size for imaging; a 2-cm long segment was isolated midway along the tail length (from 2.5 to 4.5 cm along the approximately 7-cm long tails for P21 rats) and hindlimbs were cut midway at the tibia, but otherwise were kept intact for whole-mount imaging.

A rapid micro-CT scan (standard resolution, 0.2-degree rotation and voxel size of 19 μm x 19 μm x 19 μm, which takes ~35 min to complete) was initially performed to ensure PTA stain penetration into the tissue. Once stain penetrance was verified (e.g., tendons appeared to be opaque), the tissues were then wrapped with 70% ethanol-soaked gauze and placed into 1.5 mL conical tubes. To reduce the possibility for movement artifacts during scanning, tissues were wrapped in as much gauze as needed to fill all spaces in the 1.5 mL centrifuge tube. The gauze was also saturated with 70% ethanol (for dehydrated samples) or PBS (for rehydrated samples). The 1.5 mL conical tube may be substituted with a parafilm wrap, which could reduce the space between the sample and the detector. To aid in scanning, the tissues were secured in the center of the centrifuge tube and the brass mount in as straight (i.e., vertical) an orientation as possible. The stained samples were then immediately imaged at high resolution using the micro-CT scanner (described in more detail below). Following this first set of micro-CT images, tails then underwent a serial rehydration ($n = 3$) to 100% PBS over 3 days. For serial rehydration, tissues were treated with 70% ethanol in distilled water for 1 day, then 50% ethanol in PBS for 1 day, 30% ethanol in PBS for 1 day, and lastly PBS for 1 day. These same tails were then again imaged using the micro-CT. Control tails ($n = 3$) were fixed and imaged in the scanner at the same settings as the treated samples, then dehydrated in 70% ethanol in the same manner as the PTA-stained samples, but PTA was excluded from final step, and then imaged once more. These procedures were outlined in Fig. 1.

Similar to the procedures described for P21 tails and hindlimbs, whole P50 tails ($n = 3$) and hindlimbs ($n = 3$) underwent serial dehydration over three days and then stained in 2.5% w/v PTA in 70% ethanol for 11 days. The 2.5% PTA-70% ethanol solution was changed to provide fresh solution every 3–5 days. Tails were trimmed into 2-cm long segments and hindlimbs were cut midway at the tibia and wrapped in 70% ethanol-soaked gauze and parafilm to prepare for imaging. All imaging conducted for P50 samples were at high resolution (described in more detail below).

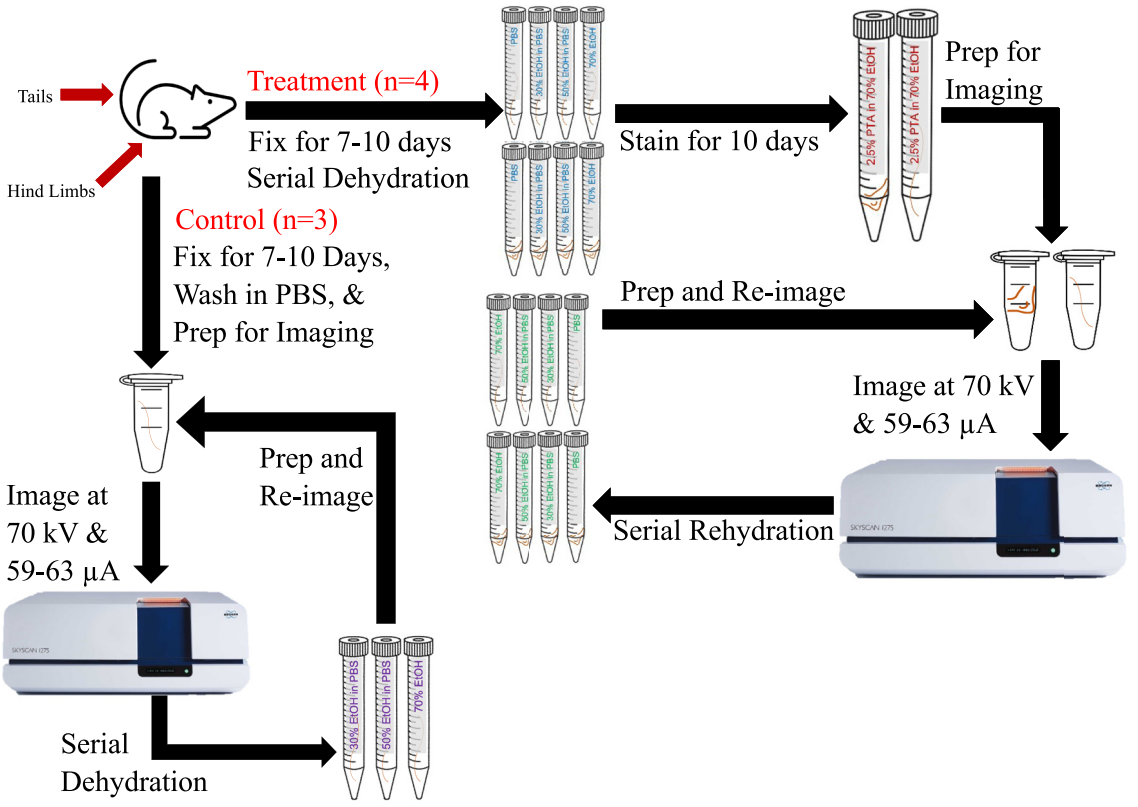

Fig. 1. Flow chart describing the method for preparation of whole-mount tissues for contrast-enhanced (and control) imaging using a micro-CT scanner.

Micro-CT imaging

A Bruker SkyScan 1275 micro-CT scanner (Bruker, Kontich, Belgium) was used for this study. Prior to each imaging session, a flat-field correction was conducted and applied using the protocol specified by the Bruker SkyScan 1275. The flat-field correction reduces image artifacts and represents the background at a similar grayscale intensity. The tissue samples were secured to the top of a brass micro-CT stand (diameter of 25 mm or 3.15 mm) with putty and the connection point was then wrapped with parafilm. All P21 samples were scanned with a 1-mm aluminum filter and the X-ray source set to a voltage of 70 kV and a current of 59–63 µA. For high resolution scans, the voxel size was 9 µm x 9 µm x 9 µm (scan time of ~1 hr and 50 min) and for standard resolution, the voxel size was 19 µm x 19 µm x 19 µm (scan time ~35 min). All P50 samples (tails) were scanned with a 1-mm aluminum filter and the X-ray source was set to a voltage of 70 kV and a current of 57–61 µA. For high resolution tail scans, the voxel size was 6.8–7 µm x 6.8–7 µm x 6.8–7 µm (scan time of ~1 hr and 50 min). For high and standard resolution scans, around 1535 or 766 transverse slices were taken with frame averaging at 5 over 360° at a rotational step of 0.1 or 0.2, respectively. Micro-CT scanner parameters (voltage, current, etc.) are provided in Supplemental Table 1 and Supplemental Table 2 and were maintained for all samples. Image reconstruction and 3D rendering was completed using NRecon (v.2.0.0.5; Bruker microCT, Kontich, Belgium) and CTvox (v.3.3; Bruker microCT, Kontich, Belgium), respectively. Fascicles were then traced manually (P21, $n = 3$ and P50, $n = 3$) based on the 3D renderings that were obtained through CTvox and individual transverse slices.

Methods validation

PTA stain and dehydration enhanced contrast of tendon

PTA stain was highly effective at improving the contrast of soft tissues to enable micro-CT imaging in 3D (Fig. 2-5). PTA-stained whole-mount tails had clearly visible soft tissues which included the six major tendon bundles that run parallel to the tail [49], the fascicles within those tendon bundles, the muscles and blood vessels, the intervertebral discs, as well as the bone within the vertebra (Fig. 2, 3a, 4, 5). The contrast-enhancing impact of PTA was most pronounced when the tissue was dehydrated in 70% ethanol. However, the contrast and tissue definition between soft tissue structures appeared to be reduced when the tissues were rehydrated in PBS. With rehydration, there is not enough contrast to clearly distinguish between the muscle, tendon, and fascicles within the tendon (Fig. 2), though the vertebra remains clearly visible. To demonstrate that it was indeed the PTA stain, and not just tissue

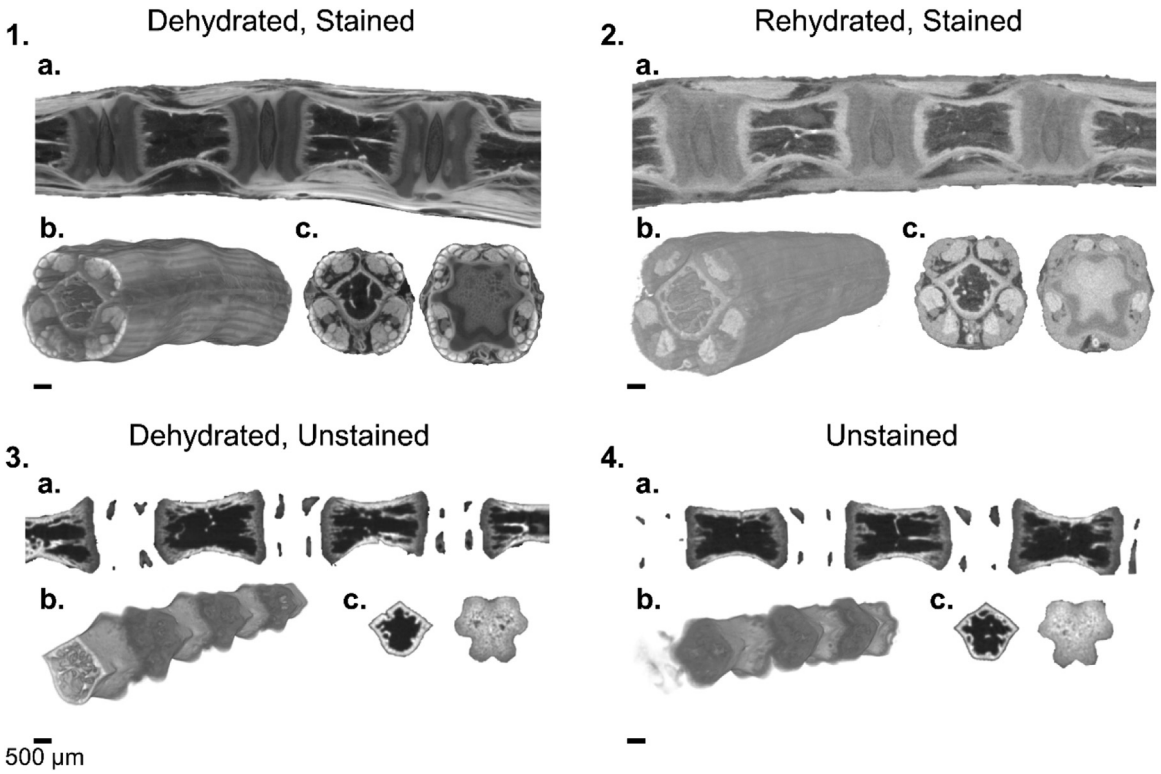

Fig. 2. 1.) Dehydrated and PTA stained P21 rat tail. **2.)** Rehydrated and PTA stained P21 rat tail. **3.)** Dehydrated and unstained P21 rat tail (dehydrated control). **4.)** Rehydrated and unstained P21 rat tail (rehydrated control). **1–4. a.)** Three dimensional micro-CT images of P21 rat tails as a function of staining and hydration. **1–4. b.)** Sagittal cross sections of rat tails **1–4. c.)** Transverse cross sections of rat tails through the center of the vertebra (left) and the start of the end plate (right). All 3D projections have a voxel size of 9 × 9 × 9 µm and the tissues are about 4.46 × 4.46 × 13.77 mm in size. (see Supplemental Table 1 for scanning parameters).

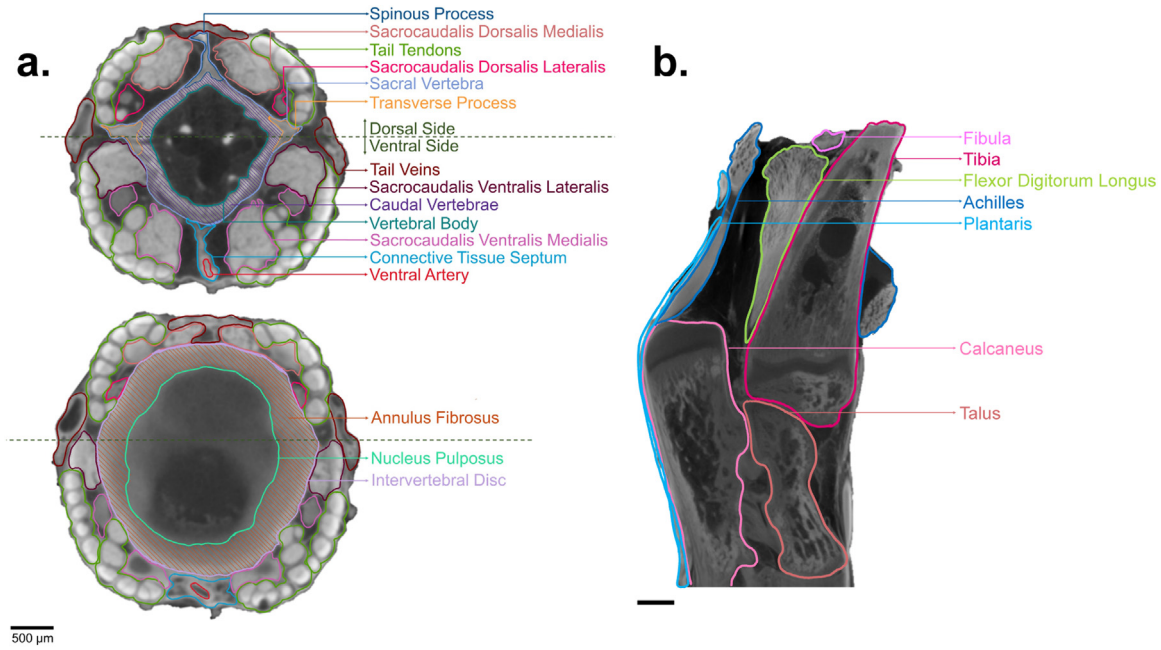

Fig. 3. a.) Transverse cross-sections of a P21 rat tail through the center of the bone and the intervertebral disc and **b.)** sagittal cross-section of a P21 rat hindlimb showing anatomical structures.

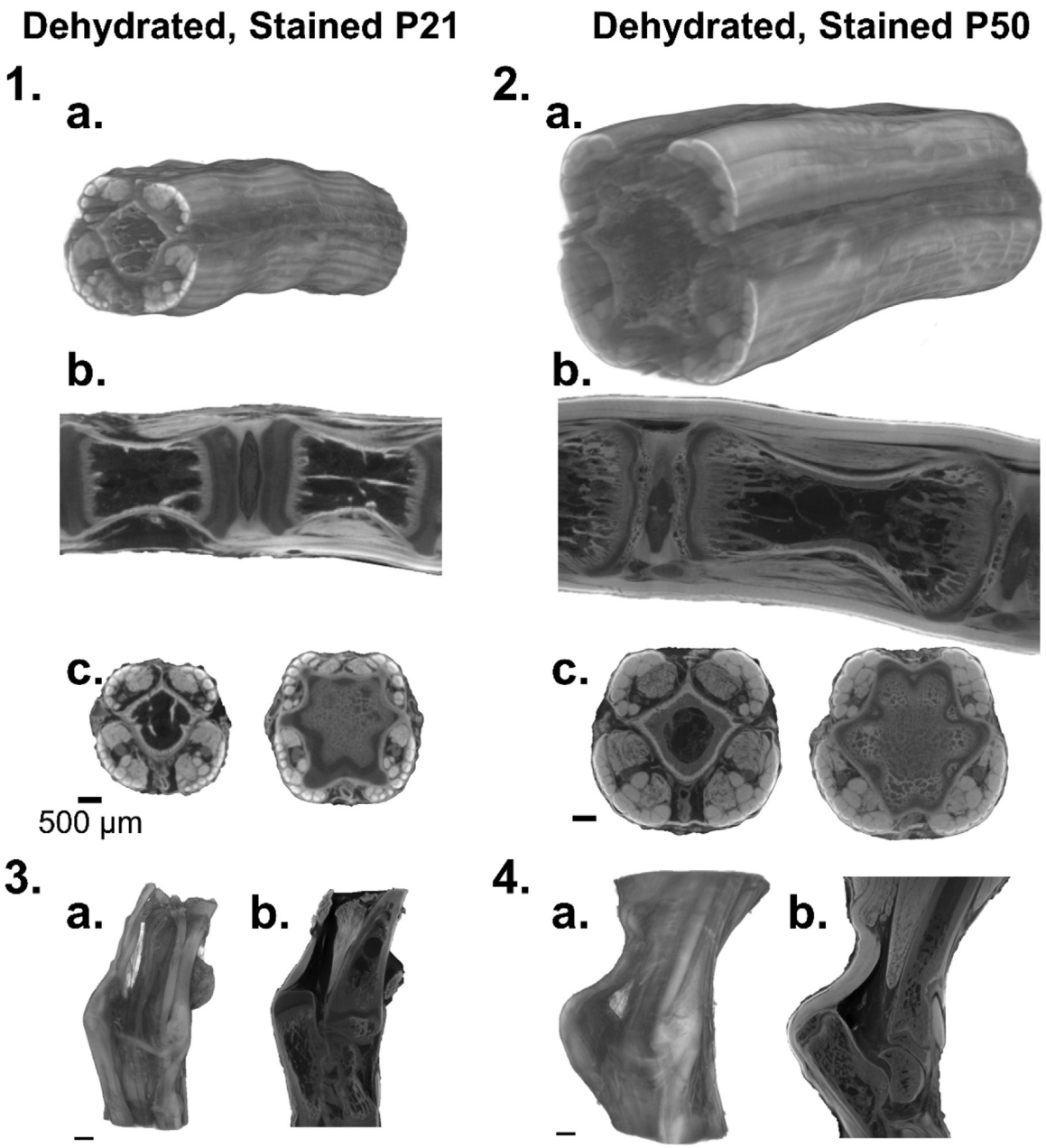

Fig. 4. 1–2. a.) Three dimensional images of rat tail midsection. **1–2. b.)** Images of sagittal tail cross-sections through the center. **1–2. c.)** Images of transverse tail cross-sections through the center of the bone (left) and the start of the end plate (right). **3–4. a.)** Three dimensional images of rat hindlimbs. **3–4. b.)** Sagittal cross-section of hindlimb. See Supplemental Table 1 & 2 for scanning parameters.

dehydration that induced high soft tissue contrast with micro-CT, unstained and dehydrated control tissues were imaged. Without PTA stain (control groups), the vertebrae were clearly visible, but there were no visible soft tissue structures in either dehydrated or rehydrated control tissues (Fig. 2), confirming that PTA stain was needed to enhance soft tissue contrast. Representative raw X-ray images (before digital reconstruction) are provided in Supplemental Figure 1, demonstrating the effectiveness of PTA and the difference in contrast between dehydrated and rehydrated samples at the same conditions.

PTA binds to the positively charged components within tissue, which suggests that ionic binding of the PTA to the highly collagenous tendon is a likely mechanism to enhance the contrast [33,50,51]. Other contrast enhancing stains like I2KI, and anionic iodine-based agents bind to complex carbohydrates like glycogen and glycosaminoglycans [46,50,52–55]. I2KI and other iodine-based stains have shown increased contrast of vasculature and skeletal muscle, but less contrast was found in highly collagenous tissues and between tissue substructures [26]. Therefore, we focused on evaluating PTA in this study to visualize the collagen-rich tendons. PMA

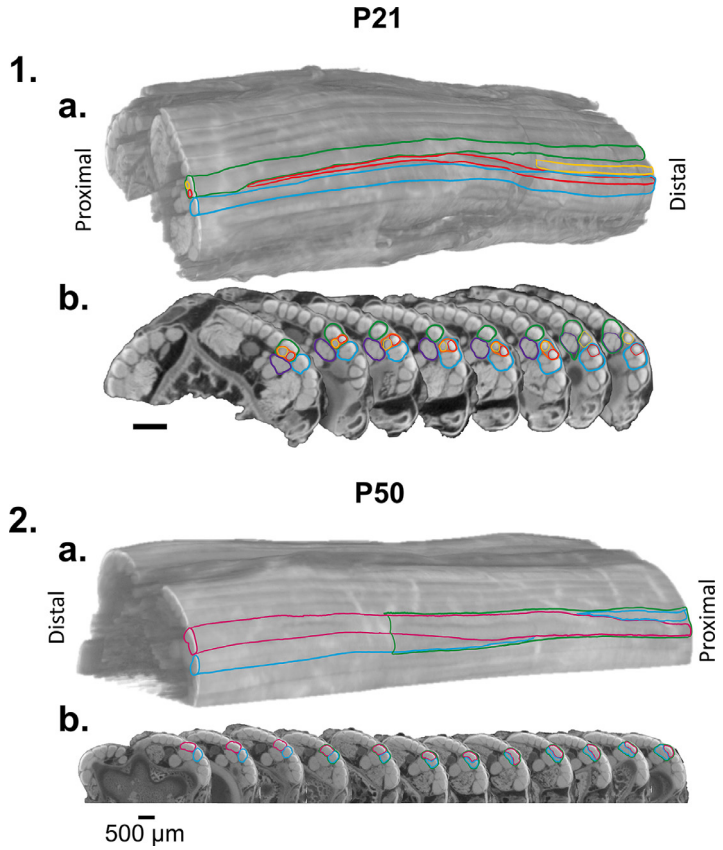

Fig. 5. 1–2. a.) Dehydrated, stained tail segment with fiber tracing (manually done) from surface of tissue and **1–2. b.)** through transverse cross sections throughout the length of the rat tail. Sub-fascicles outlined in red and yellow in 1. a-b. and pink and blue in 2. a-b. Fascicle bundles outlined in green, blue, and purple in 1. a-b. and green in 2. a-b.

was not examined due to its slow penetration time and excessive tissue shrinkage in tendon and ligament [38]. Prior studies showed that PTA has the potential to improve contrast of tendon [25,39], but it was not evaluated for different tendons types (e.g., tails and Achilles) or ages, and the impacts of tissue hydration state on image contrast were not known. Therefore, we combined aspects of prior studies with the aim to enhance contrast of tendon specifically and investigate the effect of tissue hydration.

Our study utilizes simplified serial ethanol dehydration and PBS rehydration, where other studies either used full 70% ethanol dehydrations or more extensive dehydration/rehydration steps [23,39]. It has been found that serial dehydration reduces the tissue shrinkage caused by dehydration, while increasing the soft tissue contrast. Additionally, other studies have utilized serial rehydration at lower concentrations of PTA stain (~0.7% PTA) on cranial and cartilage tissue where it was seen to increase tissue contrast [23]. Due to this, our study used rehydration steps to evaluate tissue contrast, with the goal of reducing tissue shrinkage. Other tendon studies utilized different micro-CT techniques such as phase-contrast micro-CT scanning, which is based on X-ray phase shift rather than X-ray absorption, in combination with cell maceration, critical drying, and demineralization to improve tendon visualization, but these extensive processing techniques can cause changes in the tissue structures [39]. Using Bruker CTvox software, a density gradient was applied and showed that PTA-stained tendons appeared as very high density components, even compared to the normally high density bones, where white is highest density and black is lowest density (Fig. 2-5). It is important to note that in the case of the tail tendons and Achilles and plantaris tendons, the tendons are generally more superficially located on the tail and the hindlimb. In deeper structures, stain penetration may be more limited. However, high contrast was still seen in the P50 tendons despite their much larger size, compared those at P21 (Fig. 4). Another consideration is that the tissues used in this study were obtained from relatively young animals (i.e., P21 and P50), thus tissues from much later ages might be denser as the collagen content increases and cell density decreases [56–58]. It is not known if more mature tissue will have reduced stain penetration or will have greater contrast due to their increased collagen content, but we expect that with increased staining time, the PTA will diffuse and penetrate thicker tissues. Our pilot testing with mature tissues found that this method of serial dehydration and PTA staining was still highly effective. Additionally, due to the small size of rat tendons this technique may not be directly transferrable to tendons found in much larger species, such as humans. Interestingly, rehydration reduced the tissue contrast with PTA (Fig. 2). While the exact mechanism for this loss of contrast was not determined, it is possible that rehydration played a role in washing out the PTA, as it is water soluble [51]. Our own pilot testing found that if the samples are stored in 70% ethanol after PTA staining, they can be reimaged nearly one year

later and retain their high tendon contrast. The hindlimbs were not rehydrated, due to the reduced contrast found in the rehydrated tails. Further, there was no visually observed change in overall tissue size between the PTA-stained and dehydrated tissues, compared to the rehydrated tissues, suggesting that there was limited change in the overall tissue architecture.

Identification of soft tissues was possible in PTA stained and dehydrated tails and hindlimbs

PTA-staining and dehydration improved contrast between tissues and maintained anatomical details so that the tissue components and substructures are clearly identifiable in tails and hindlimbs (Fig. 3). Due to the high contrast in the tail, the muscles, blood vessels, as well as substructures in the intervertebral disc (nucleus pulposus, annulus fibrosis) and tendon (larger diameter sub-fascicles, fascicles, and tertiary fiber bundles) could be visualized (Fig. 3a and 5). In the hindlimb, the three main bundles that make up the Achilles were identified along with their insertion into the calcaneus, as well as the plantaris tendon. (Fig. 3b). Though beyond the scope of this study, investigators could then use image analysis to quantify typically evaluated size factors such as tissue length, diameter, and cross-sectional area, as well as relative density, and relationships between adjacent tissues (distances, location of insertion sites, etc.). Micro-CT is commonly used to evaluate changes in bone with respect to mechanical stimuli, genotype, age, and many others [59–61]. This method provides a new option to include soft tissues into these investigations of the bony anatomy when conducting *ex vivo* analysis.

To visualize anatomy at the microscale, histology is commonly used and typically involves tissue fixation, sectioning a 3D tissue into thin 2D slices, mounting sections on slides, staining with hematoxylin and eosin, and then imaging on a microscope [23,62]. Histology has its advantages, mainly the ability to visualize cell-level details, allows for immunolabeling for detecting specific proteins, and is appropriate for several applications, but there are some limitations. These limitations include the time and labor-intensive tissue processing that is prone to artifact from the sectioning process and the challenge of sectioning, imaging, and rendering the physical 2D slices into a 3D image [22,24]. These challenges limit the tissue processing to relatively small tissues or small sections of larger tissues. While PTA tissue staining takes time (here the tissue was stained for 10 days to ensure penetration into the whole-mount tissues) and is currently unable to image the fibril and smaller fiber levels, the staining and tissue processing is much less labor intensity, compared to histology, and has reduced potential tissue damage since the tissue can be maintained relatively intact (only the skin was removed in our study) [13,23]. Lastly, as micro-CT is non-destructive, the tissues are still intact after imaging possibility enabling additional analysis, including but not limited to re-imaging. These analyses would be limited to those that require chemical tissue fixation.

Contrast-enhanced micro-CT imaging enabled tail tendon fascicle tracking in 3D

The 3D micro-CT images of the tails enabled the visualization of the tail tendon fascicles over relatively long distances (~ 1 cm) along the length of the tail sections (Fig. 5). From the micro-CT slices and 3D representations of the tissue, the tendon fascicles were traced from one end of the tail section to the opposing end (Fig. 5). Tendon sub-fascicle bundles were observed crossing over one another and joining different fascicle bundles and separating from their original fascicle bundles and forming new fascicle bundles along the length of the tail section. This was a particularly surprising finding since it has been assumed that the fascicle bundles maintain specific tracks within the tendon. This fascicle crossover was not only present in immature animals (P21) ($n = 3$), but also in more mature animals (P50) ($n = 3$). Single sub-fascicles crossing from and joining different fascicle bundles was only observed in P21 samples ($n = 1$), however, large fascicle bundles separating into smaller bundles was observed in each sample (P21 $n = 3$, P50 $n = 3$). Future studies will be needed to identify what role these fascicle bundles that crossover play in moving the tail, but given that the tail contains 31–36 vertebrae, and 6 major tendon bundles [49,63,64], it is possible that this fascicle crossover provides control or stabilization of specific tail segments. This initial finding shows that micro-CT imaging of contrast-enhanced tendon is effective enough to track individual tendon substructures and how they change throughout the length of the tissue. To determine the full extent of this crossover throughout the whole length of the tail and in all six major tendons, future in-depth studies that employ fiber tracing algorithms will be needed [43,65–68].

Future applications

The proposed micro-CT imaging technique for tails and hindlimbs has numerous potential future applications. Changes in tendon structure, such as fascicle size, distribution, and density, as a function of age can be evaluated since we showed this staining methodology is effective at both early (e.g., P21) and later (e.g., P50) ages. Future studies will compare tendon structure across these and other stages of development. Additionally, this imaging technique can be utilized to study the variations in tendon structure between different tendon types (e.g. Achilles vs. tails) and between different species (e.g., mice, rats, rabbit, etc.). By readily imaging both the bone and soft tissues in 3D, another potential application is the evaluation of the insertion sites of tendon into bone and their corresponding muscle groups to better understand the bone-tendon-muscle connections throughout development. The proposed method can also be applied to study the various micro- and macro-structures (fibers, sub-fascicles, fascicles, sub-tendon, etc.) and their arrangements within the whole tendon. Ultimately, future studies that couple this methodology with image segmentation and fiber tracing algorithms will elucidate fascicle and sub-fascicle arrangement and organization throughout the entirety of a tissue sample or limb. This will aid future studies to determine structure-function relationships in tendon and help to answer questions on tendon fascicle architecture and control of limb positioning.

Conclusion

In conclusion, we highlighted a simple method for visualizing tendon by micro-CT. PTA staining in ethanol increased X-ray absorption by tendon, increasing their contrast, to obtain 3D micro-CT images at high enough resolution to visualize and trace sub-fascicles in the tail tendon. This method was demonstrated on both immature (postnatal day 21) and sexually mature (postnatal day 50) rat tendons within the tail and hindlimb. Further, we showed that the impact of PTA-induced soft tissue contrast is diminished if the tissues are rehydrated in PBS. Using this visualization method, future studies can determine structure-function relationships in tendon, tendon sub-fascicle and fascicle architecture and organization, and tendon interactions with surrounding tissues and bone.

Ethics statements

All animal experiments complied with ARRIVE guidelines and were carried out in accordance with the National Institutes of Health guide for the care and use of laboratory animals (NIH Publications No. 8023, revised 1978).

Declaration of Competing Interest

The authors declare that they have no known competing financial interests or personal relationships that could have appeared to influence the work reported in this paper.

CRediT authorship contribution statement

Destinee M. Ditton: Conceptualization, Methodology, Data curation, Writing – original draft, Writing – review & editing. **Colin R. Marchus:** Methodology, Writing – original draft, Writing – review & editing. **Aimee L. Bozeman:** Methodology, Data curation, Writing – review & editing. **Alleyna C. Martes:** Methodology, Data curation, Writing – review & editing. **Michele R. Brumley:** Conceptualization, Methodology, Supervision, Writing – review & editing. **Nathan R. Schiele:** Supervision, Conceptualization, Methodology, Writing – original draft, Writing – review & editing.

Data availability

Data will be made available on request.

Acknowledgments

This publication was made possible by the INBRE Program, NIH Grant No. P20 GM103408, micro-CT scanner SkyScan 1275 that was sponsored by the Murdock Charitable Trust in the University of Idaho 3D Imaging and Printing Laboratory, and the University of Idaho Office of Undergraduate Research.

Supplementary materials

Supplementary material associated with this article can be found, in the online version, at doi:10.1016/j.mex.2024.102565.

References

[1] J.D. Boerckel, D.E. Mason, A.M. McDermott, E. Alsberg, Microcomputed tomography: approaches and applications in bioengineering, Stem Cell Res. Ther. 5 (2014) 144, doi:10.1186/scrt534.
[2] M.L. Bouxsein, S.K. Boyd, B.A. Christiansen, R.E. Guldberg, K.J. Jepsen, R. Müller, Guidelines for assessment of bone microstructure in rodents using micro-computed tomography, J. Bone Miner. Res. 25 (2010) 1468–1486, doi:10.1002/jbmr.141.
[3] D.P. Clark, C.T. Badea, Micro-CT of rodents: state-of-the-art and future perspectives, Physica Med. 30 (2014) 619–634, doi:10.1016/j.ejmp.2014.05.011.
[4] Y. Kim, M.D. Brodt, S.Y. Tang, M.J. Silva, MicroCT for scanning and analysis of mouse bones, in: M.J. Hilton (Ed.), Skeletal Development and Repair, Springer US, New York, NY, 2021, pp. 169–198, doi:10.1007/978-1-0716-1028-2_11.
[5] R.E. Guldberg, R.T. Ballock, B.D. Boyan, C.L. Duvall, A.S.P. Lin, S. Nagaraja, M. Oest, J. Phillips, B.D. Porter, G. Robertson, W.R. Taylor, Analyzing bone, blood vessels, and biomaterials with microcomputed tomography, IEEE Eng. Med. Biol. Mag. 22 (2003) 77–83, doi:10.1109/MEMB.2003.1256276.
[6] R. Müller, Hierarchical microimaging of bone structure and function, Nat. Rev. Rheumatol. 5 (2009) 373–381, doi:10.1038/nrrheum.2009.107.
[7] M. Stauber, R. Müller, Micro-Computed tomography: a method for the non-destructive evaluation of the three-dimensional structure of biological specimens, in: J.J. Westendorf (Ed.), Osteoporosis, Humana Press, Totowa, NJ, 2008, pp. 273–292, doi:10.1007/978-1-59745-104-8_19.
[8] D.L. Batiste, A. Kirkley, S. Laverty, L.M.F. Thain, A.R. Spouge, D.W. Holdsworth, Ex vivo characterization of articular cartilage and bone lesions in a rabbit ACL transection model of osteoarthritis using MRI and micro-CT, Osteoarthritis Cartilage 12 (2004) 986–996, doi:10.1016/j.joca.2004.08.010.
[9] H.R. Buie, G.M. Campbell, R.J. Klinck, J.A. MacNeil, S.K. Boyd, Automatic segmentation of cortical and trabecular compartments based on a dual threshold technique for in vivo micro-CT bone analysis, Bone 41 (2007) 505–515, doi:10.1016/j.bone.2007.07.007.
[10] D. Cooper, A. Turinsky, C. Sensen, B. Hallgrimsson, Effect of voxel size on 3D micro-CT analysis of cortical bone porosity, Calcif. Tissue Int. 80 (2007) 211–219, doi:10.1007/s00223-005-0274-6.
[11] E. Perilli, A.M. Briggs, S. Kantor, J. Codrington, J.D. Wark, I.H. Parkinson, N.L. Fazzalari, Failure strength of human vertebrae: prediction using bone mineral density measured by DXA and bone volume by micro-CT, Bone 50 (2012) 1416–1425, doi:10.1016/j.bone.2012.03.002.
[12] B.D. Metscher, MicroCT for comparative morphology: simple staining methods allow high-contrast 3D imaging of diverse non-mineralized animal tissues, BMC Physiol. 9 (2009) 11, doi:10.1186/1472-6793-9-11.
[13] B.D. Metscher, MicroCT for developmental biology: a versatile tool for high-contrast 3D imaging at histological resolutions, Dev. Dyn. 238 (2009) 632–640, doi:10.1002/dvdy.21857.

[14] G.G. Handsfield, L.C. Slane, H.R.C. Screen, Nomenclature of the tendon hierarchy: an overview of inconsistent terminology and a proposed size-based naming scheme with terminology for multi-muscle tendons, J. Biomech. 49 (2016) 3122–3124, doi:10.1016/j.jbiomech.2016.06.028.
[15] C.T. Thorpe, P.D. Clegg, H.L. Birch, A review of tendon injury: why is the equine superficial digital flexor tendon most at risk?: why is the equine superficial digital flexor tendon most at risk? Equine Vet. J. 42 (2010) 174–180, doi:10.2746/042516409X480395.
[16] F.H. Silver, J.W. Freeman, G.P. Seehra, Collagen self-assembly and the development of tendon mechanical properties, J. Biomech. 36 (2003) 1529–1553, doi:10.1016/S0021-9290(03)00135-0.
[17] P. Kannus, Structure of the tendon connective tissue: tendon connective tissue structure, Scand. J. Med. Sci. Sports 10 (2000) 312–320, doi:10.1034/j.1600-0838.2000.010006312.x.
[18] J. Kastelic, A. Galeski, E. Baer, The multicomposite structure of tendon, Connect. Tissue Res. 6 (1978) 11–23, doi:10.3109/03008207809152283.
[19] M. Franchi, A. Trirè, M. Quaranta, E. Orsini, V. Ottani, Collagen structure of tendon relates to function, Sci. World J. 7 (2007) 404–420, doi:10.1100/tsw.2007.92.
[20] J.H.-C. Wang, Mechanobiology of tendon, J. Biomech. 39 (2006) 1563–1582, doi:10.1016/j.jbiomech.2005.05.011.
[21] A.H. Lee, D.M. Elliott, Comparative multi-scale hierarchical structure of the tail, plantaris, and Achilles tendons in the rat, J. Anat. 234 (2019) 252–262, doi:10.1111/joa.12913.
[22] D.W. Holdsworth, M.M. Thornton, Micro-CT in small animal and specimen imaging, Trends Biotechnol. 20 (2002) S34–S39, doi:10.1016/S0167-7799(02)02004-8.
[23] K.M. Lesciotto, S.M. Motch Perrine, M. Kawasaki, T. Stecko, T.M. Ryan, K. Kawasaki, J.T. Richtsmeier, Phosphotungstic acid-enhanced microCT: optimized protocols for embryonic and early postnatal mice, Dev. Dyn. 249 (2020) 573–585, doi:10.1002/dvdy.136.
[24] F.J. Rühli, G. Kuhn, R. Evison, R. Müller, M. Schultz, Diagnostic value of micro-CT in comparison with histology in the qualitative assessment of historical human skull bone pathologies, Am. J. Phys. Anthropol. 133 (2007) 1099–1111, doi:10.1002/ajpa.20611.
[25] E. Pauwels, D. Van Loo, P. Cornillie, L. Brabant, L. Van Hoorebeke, An exploratory study of contrast agents for soft tissue visualization by means of high resolution X-ray computed tomography imaging: contrast agents for soft tissue visualization with microct, J. Microsc. 250 (2013) 21–31, doi:10.1111/jmi.12013.
[26] C.M. Disney, K. Madi, A.J. Bodey, P.D. Lee, J.A. Hoyland, M.J. Sherratt, Visualising the 3D microstructure of stained and native intervertebral discs using X-ray microtomography, Sci. Rep. 7 (2017) 16279, doi:10.1038/s41598-017-16354-w.
[27] J. Dudak, J. Zemlicka, J. Karch, M. Patzelt, J. Mrzilkova, P. Zach, Z. Hermanova, J. Kvacek, F. Krejci, High-contrast X-ray micro-radiography and micro-CT of ex-vivo soft tissue murine organs utilizing ethanol fixation and large area photon-counting detector, Sci. Rep. 6 (2016) 30385, doi:10.1038/srep30385.
[28] K. Degenhardt, A.C. Wright, D. Horng, A. Padmanabhan, J.A. Epstein, Rapid 3D phenotyping of cardiovascular development in mouse embryos by micro-CT with iodine staining, Cardiovascular Imaging 3 (2010) 314–322, doi:10.1161/CIRCIMAGING.109.918482.
[29] P.M. Gignac, N.J. Kley, Iodine-enhanced micro-CT imaging: methodological refinements for the study of the soft-tissue anatomy of post-embryonic vertebrates: iodine-enhanced μCT imaging of vertebrates, J. Exp. Zool. (Mol. Dev. Evol.). 322 (2014) 166–176, doi:10.1002/jez.b.22561.
[30] N.S. Jeffery, R.S. Stephenson, J.A. Gallagher, J.C. Jarvis, P.G. Cox, Micro-computed tomography with iodine staining resolves the arrangement of muscle fibres, J Biomech 44 (2011) 189–192, doi:10.1016/j.jbiomech.2010.08.027.
[31] M. Nierenberger, Y. Rémond, S. Ahzi, P. Choquet, Assessing the three-dimensional collagen network in soft tissues using contrast agents and high resolution micro-CT: application to porcine iliac veins, C. R. Biol. 338 (2015) 425–433, doi:10.1016/j.crvi.2015.04.009.
[32] T. Shearer, R.S. Bradley, L.A. Hidalgo-Bastida, M.J. Sherratt, S.H. Cartmell, Three-dimensional visualisation of soft biological structures by X-ray computed micro-tomography, J. Cell. Sci. (2016) jcs.179077, doi:10.1242/jcs.179077.
[33] V.S. Constantine, R.W. Mowry, Selective staining of human dermal collagen, J. Invest. Dermatol. 50 (1968) 419–423, doi:10.1038/jid.1968.68.
[34] P. Das Neves Borges, A.E. Forte, T.L. Vincent, D. Dini, M. Marenzana, Rapid, automated imaging of mouse articular cartilage by microCT for early detection of osteoarthritis and finite element modelling of joint mechanics, Osteoarthritis Cartilage 22 (2014) 1419–1428, doi:10.1016/j.joca.2014.07.014.
[35] S. Faulwetter, T. Dailianis, A. Vasileiadou, C. Arvanitidis, Contrast enhancing techniques for the application of micro-CT in marine biodiversity studies, Comput. Tomography (2013).
[36] M.L. Watson, Staining of Tissue Sections for Electron Microscopy with Heavy Metals, (n.d.).
[37] H.J. Nieminen, T. Ylitalo, S. Karhula, J.P. Suuronen, S. Kauppinen, R. Serimaa, E. Hæggström, K.P.H. Pritzker, M. Valkealahti, P. Lehenkari, M. Finnilä, S. Saarakkala, Determining collagen distribution in articular cartilage using contrast-enhanced micro-computed tomography, Osteoarthritis Cartilage 23 (2015) 1613–1621, doi:10.1016/j.joca.2015.05.004.
[38] R. Balint, T. Lowe, T. Shearer, Optimal contrast agent staining of ligaments and tendons for X-Ray computed tomography, PLoS ONE 11 (2016) e0153552, doi:10.1371/journal.pone.0153552.
[39] J. Sartori, S. Köhring, H. Witte, M.S. Fischer, M. Löffler, Three-dimensional imaging of the fibrous microstructure of Achilles tendon entheses in Mus musculus, J. Anat. 233 (2018) 370–380, doi:10.1111/joa.12837.
[40] J. Buytaert, J. Goyens, D. De Greef, P. Aerts, J. Dirckx, Volume shrinkage of bone, brain and muscle tissue in sample preparation for Micro-CT and light sheet fluorescence microscopy (LSFM), Microsc. Microanal. 20 (2014) 1208–1217, doi:10.1017/S1431927614001329.
[41] M. Kaucka, J. Petersen, M. Tesarova, B. Szarowska, M.E. Kastriti, M. Xie, A. Kicheva, K. Annusver, M. Kasper, O. Symmons, L. Pan, F. Spitz, J. Kaiser, M. Hovorakova, T. Zikmund, K. Sunadome, M.P. Matise, H. Wang, U. Marklund, H. Abdo, P. Ernfors, P. Maire, M. Wurmser, A.S. Chagin, K. Fried, I. Adameyko, Signals from the brain and olfactory epithelium control shaping of the mammalian nasal capsule cartilage, Elife 7 (2018) e34465, doi:10.7554/eLife.34465.
[42] D. De Greef, J.A.N. Buytaert, J.R.M. Aerts, L. Van Hoorebeke, M. Dierick, J. Dirckx, Details of human middle ear morphology based on micro-CT imaging of phosphotungstic acid stained samples: human middle ear morphology through micro-CT, J. Morphol. 276 (2015) 1025–1046, doi:10.1002/jmor.20392.
[43] N. Marr, M. Hopkinson, A.P. Hibbert, A.A. Pitsillides, C.T. Thorpe, Bimodal whole-mount imaging of tendon using confocal microscopy and x-ray micro-computed tomography, Biol. Proced. Online 22 (2020) 13, doi:10.1186/s12575-020-00126-4.
[44] N.R. Council, Guide For the Care and Use of Laboratory Animals: Eighth Edition, The National Academies Press, Washington, DC, 2011, doi:10.17226/12910.
[45] M. Sonnaert, G. Kerckhofs, I. Papantoniou, S. Van Vlierberghe, V. Boterberg, P. Dubruel, F.P. Luyten, J. Schrooten, L. Geris, Multifactorial optimization of contrast-enhanced nanofocus computed tomography for quantitative analysis of neo-tissue formation in tissue engineering constructs, PLoS ONE 10 (2015) e0130227, doi:10.1371/journal.pone.0130227.
[46] E. Descamps, A. Sochacka, B. De Kegel, D. Van Loo, L. Van Hoorebeke, D. Adriaens, Soft tissue discrimination with contrast agents using micro-CT scanning, Belg. J. Zool. (2020) 144, doi:10.26496/bjz.2014.63.
[47] M. Kaucka, T. Zikmund, M. Tesarova, D. Gyllborg, A. Hellander, J. Jaros, J. Kaiser, J. Petersen, B. Szarowska, P.T. Newton, V. Dyachuk, L. Li, H. Qian, A.S. Johansson, Y. Mishina, J.D. Currie, E.M. Tanaka, A. Erickson, A. Dudley, H. Brismar, P. Southam, E. Coen, M. Chen, L.S. Weinstein, A. Hampl, E. Arenas, A.S. Chagin, K. Fried, I. Adameyko, Oriented clonal cell dynamics enables accurate growth and shaping of vertebrate cartilage, Elife 6 (2017) e25902, doi:10.7554/eLife.25902.
[48] B.D. Metscher, X-Ray microtomographic imaging of intact vertebrate embryos, Cold Spring Harb. Protoc. 2011 (2011) pdb.prot067033, doi:10.1101/pdb.prot067033.
[49] A. Bruneau, N. Champagne, P. Cousineau-Pelletier, G. Parent, E. Langelier, Preparation of rat tail tendons for biomechanical and mechanobiological studies, J. Vis. Exp. (2010) 2176, doi:10.3791/2176.
[50] L. Silverman, D. Glick, The reactivity and staining of tissue proteins with phosphotungstic acid, J. Cell Biol. 40 (1969) 761–767, doi:10.1083/jcb.40.3.761.
[51] I. Leizerman, 26010747.nbib, (2005). http://www.wetsem.com/tec_lit/PTAstainingftissue.pdf.
[52] J.A. McCaul, J.A. Cymerman, S. Hislop, C. McConkey, J. McMahon, H. Mehanna, R. Shaw, D.N. Sutton, J. Dunn, LIHNCS - Lugol's iodine in head and neck cancer surgery: a multicentre, randomised controlled trial assessing the effectiveness of Lugol's iodine to assist excision of moderate dysplasia, severe dysplasia and carcinoma in situ at mucosal resection margins of oral and oropharyngeal squamous cell carcinoma: study protocol for a randomised controlled trial, Trials 14 (2013) 310, doi:10.1186/1745-6215-14-310.
[53] P.N. Bansal, R.C. Stewart, V. Entezari, B.D. Snyder, M.W. Grinstaff, Contrast agent electrostatic attraction rather than repulsion to glycosaminoglycans affords a greater contrast uptake ratio and improved quantitative CT imaging in cartilage, Osteoarthritis Cartilage 19 (2011) 970–976, doi:10.1016/j.joca.2011.04.004.

[54] P.N. Bansal, N.S. Joshi, V. Entezari, B.C. Malone, R.C. Stewart, B.D. Snyder, M.W. Grinstaff, Cationic contrast agents improve quantification of glycosaminoglycan (GAG) content by contrast enhanced CT imaging of cartilage, J. Orthop. Res. 29 (2011) 704–709, doi:10.1002/jor.21312.
[55] M.D. Newton, S.E. Hartner, S. Timmons, N.D. Delaney, M.G. Pirrone, K.C. Baker, T. Maerz, Contrast-enhanced μCT of the intervertebral disc: a comparison of anionic and cationic contrast agents for biochemical and morphological characterization: Contrast-Enhanced μCT of the IVD, J. Orthop. Res. 35 (2017) 1067–1075, doi:10.1002/jor.23364.
[56] J.E. Marturano, J.D. Arena, Z.A. Schiller, I. Georgakoudi, C.K. Kuo, Characterization of mechanical and biochemical properties of developing embryonic tendon, Proc. Natl. Acad. Sci. USA 110 (2013) 6370–6375, doi:10.1073/pnas.1300135110.
[57] R. Meller, F. Schiborra, G. Brandes, K. Knobloch, T. Tschernig, S. Hankemeier, C. Haasper, A. Schmiedl, M. Jagodzinski, C. Krettek, E. Willbold, Postnatal maturation of tendon, cruciate ligament, meniscus and articular cartilage: a histological study in sheep, Annals of Anatomy - Anatomischer Anzeiger 191 (2009) 575–585, doi:10.1016/j.aanat.2009.08.005.
[58] S.K. Theodossiou, N.R. Schiele, Models of tendon development and injury, BMC Biomed. Eng. 1 (2019) 32, doi:10.1186/s42490-019-0029-5.
[59] M.M. Hurley, Y. Okada, L. Xiao, Y. Tanaka, M. Ito, N. Okimoto, T. Nakamura, C.J. Rosen, T. Doetschman, J.D. Coffin, Impaired bone anabolic response to parathyroid hormone in Fgf2−/− and Fgf2+/− mice, Biochem. Biophys. Res. Commun. 341 (2006) 989–994, doi:10.1016/j.bbrc.2006.01.044.
[60] I.S. Maggiano, C.M. Maggiano, J.G. Clement, C.D.L. Thomas, Y. Carter, D.M.L. Cooper, Three-dimensional reconstruction of Haversian systems in human cortical bone using synchrotron radiation-based micro-CT: morphology and quantification of branching and transverse connections across age, J. Anat. 228 (2016) 719–732, doi:10.1111/joa.12430.
[61] F.A. Schulte, D. Ruffoni, F.M. Lambers, D. Christen, D.J. Webster, G. Kuhn, R. Müller, Local mechanical stimuli regulate bone formation and resorption in mice at the tissue level, PLoS ONE 8 (2013) e62172, doi:10.1371/journal.pone.0062172.
[62] H.A. Alturkistani, F.M. Tashkandi, Z.M. Mohammedsaleh, Histological stains: a literature review and case study, GJHS 8 (2015) 72, doi:10.5539/gjhs.v8n3p72.
[63] M.A. Olude, O.A. Mustapha, T.K. Ogunbunmi, J.O. Olopade, The vertebral column, ribs, and sternum of the african giant rat (Cricetomys gambianus waterhouse), Sci. World J. 2013 (2013) 1–5, doi:10.1155/2013/973537.
[64] R.L. Maynard, N. Downes, in: Vertebrae, Ribs, Sternum, Pectoral and Pelvic Girdles, and Bones of the Limbs, in: Anatomy and Histology of the Laboratory Rat in Toxicology and Biomedical Research, Elsevier, 2019, pp. 23–39, doi:10.1016/B978-0-12-811837-5.00004-6.
[65] C.N. Eberhardt, A.R. Clarke, Automated reconstruction of curvilinear fibres from 3D datasets acquired by X-ray microtomography, J. Microsc. 206 (2002) 41–53, doi:10.1046/j.1365-2818.2002.01009.x.
[66] M. Reichardt, M. Töpperwien, A. Khan, F. Alves, T. Salditt, Fiber orientation in a whole mouse heart reconstructed by laboratory phase-contrast micro-CT, J. Med. Imag. 7 (2020) 1, doi:10.1117/1.JMI.7.2.023501.
[67] J. Sartori, H. Stark, Tracking tendon fibers to their insertion – a 3D analysis of the Achilles tendon enthesis in mice, Acta Biomater. 120 (2021) 146–155, doi:10.1016/j.actbio.2020.05.001.
[68] S.P. Sullivan, F.R. McGechie, K.M. Middleton, C.M. Holliday, 3D muscle architecture of the pectoral muscles of european starling (Sturnus vulgaris), Integr. Org. Biol. 1 (2019) oby010, doi:10.1093/iob/oby010.